Anion Radicals of Mono- and Bisfulleropyrrolidines: g Tensors, Spin Density Distribution and Spin−Lattice Relaxation

Alfonso Zoleo,[†] Anna Lisa Maniero,[†] Maurizio Prato,[‡] Maria Gabriella Severin,[†] Louis Claude Brunel,[§] Konstantinos Kordatos,[‡] and Marina Brustolon*,[†]

Dipartimento di Chimica Fisica, Universitá di Padova, Via Loredan 2, I-35131 Padova, Italy, and Dipartimento di Scienze Farmaceutiche, Universitá di Trieste, Piazzale Europa, 34100 Trieste, Italy, and Center for Interdisciplinary Magnetic Resonance, National High Magnetic Field Laboratory, Florida State University, Tallahassee, Florida 32306

Received: April 20, 2000; In Final Form: July 25, 2000

The radical anions of two C_{60} Nteg-fulleropyrrolidine (teg = 3,6,9-trioxadecyl) adducts, the monoadduct and the trans1-bisadduct have been studied in liquid solution and glassy matrix of 2-MeTHF by continuous wave (cw) and pulsed X-band EPR and cw high-frequency EPR. The hyperfine coupling constants of the ^{14}N nuclei and of the ^{13}C nuclei in natural abundance have been determined and discussed, also in relation with the spin density distribution on the fullerene sphere obtained by restricted Hartree−Fock half-electron approximation (RHF-HE), and the hyperfine coupling constants obtained with the density functional method. The calculation results show a reasonable agreement with the experimental data. The **g** tensors have been determined by HF-EPR in frozen matrix at low temperature, the monoadduct showing a rhombic tensor and the bisadduct an axial one. The temperature dependence of the EPR line widths and of the electron spin−lattice relaxation times measured by Inversion Recovery of the magnetization have been studied. The radical anion of the bisadduct shows line widths decreasing on increasing the temperature, as usually expected, whereas the radical anion of the monoadduct shows the opposite behavior. The electron spin−lattice relaxation times at room temperature are respectively $T_1 = 2.8$ μs and $T_1 = 200$ ns. The relaxation behavior has been discussed and compared with that of the C_{60} monoanion and of other fulleropyrrolidine adducts, taking into account the time modulation of the parameters of the spin Hamiltonian due to the reorientation in solution, and the coupling between rotational and electron spin magnetic moments. This spin-rotational mechanism gives rise to the short T_1 and anomalous temperature dependence of the line widths in the monoadduct, whereas the larger stiffness of the bisadduct reduces this effect.

Introduction

The paramagnetic species produced by reduction of C_{60} and some of its derivatives have been extensively studied with EPR in the past years.[1−15] A comprehensive review on fulleride anions and fullerenium cations has been recently published (see ref 16, and references therein).

An interesting class of fullerene derivatives is that of the fulleropyrrolidines (FP), prepared by 1,3-dipolar cycloaddition of azomethine ylides to C_{60}.[17] This methodology provides a broad variety of useful functionalized fullerenes, produced with practical applications as the scope.[18] In particular, elucidation of the electronic structure of reduced fulleropyrrolidines becomes important as these compounds are extensively used as electron-accepting units in electro- and photoactive diads.[19] In a recent cw and pulsed EPR study[20] we have shown that the EPR spectra of the radical anions of FP show some interesting features, that give a better insight into their structure than similar studies for many other fullerene derivatives.

In fact in general the radical anions of fullerene derivatives in their EPR spectra show a single line, lacking any hyperfine structure. On the other hand, in the case of FP radical anions the spectra show a hyperfine structure due to the interaction of the unpaired electron with the ^{14}N nucleus, and satellite lines due to the anions bearing a ^{13}C in some position of the bucky ball. From these data one can obtain an useful information on the spin distribution on the π system and on its symmetry. Moreover, the temperature dependence of the EPR line widths, and the direct measure of T_1 with pulsed EPR experiments, have shown that the FP radical anions have in general a spin−lattice relaxation time much shorter than ordinary radicals. This effect is known to be typical of fullerene derivatives, the T_1 value being very short for C_{60}^- (∼1 ns at room temperature), and then increasing in monoadducts (for example ∼100 ns for *N*-methylfulleropyrrolidine$^-$) and still increasing in bisadducts (∼1 μs for bis-*N*-methyl-3,4-fulleropyrrolidine$^-$).

The short T_1 has been attributed to the near degeneracy of the π-electrons energy levels of fullerenes, allowing fast radiationless transitions between the different electronic states.

In this paper we report a continuous wave X-band and W-band, and pulsed X-band EPR study, on the radical anions of two pyrrolidine adducts, the monoadduct NTEG and the bisadduct TRANS1 (see Scheme 1).

[†] Universita di Padova. E-mail addresses: zoleo@corgia.chfi.unipd.it, a.l.maniero@chfi.unipd.it, M.G.Severin@chfi.unipd.it, M.Brustolon@chfi.unipd.it. Fax: +39-049-8275135.

[‡] Universitá di Trieste. E-mail addresses: prato@univ.trieste.it, kordatos@univ.trieste.it. Fax: +39-040-52572.

[§] Florida State University. E-mail: L. C. Brunel brunel@magnet.fsu.edu. Fax: +1-850-644-1366.

10.1021/jp001518s CCC: $19.00
Published on Web 10/13/2000

SCHEME 1

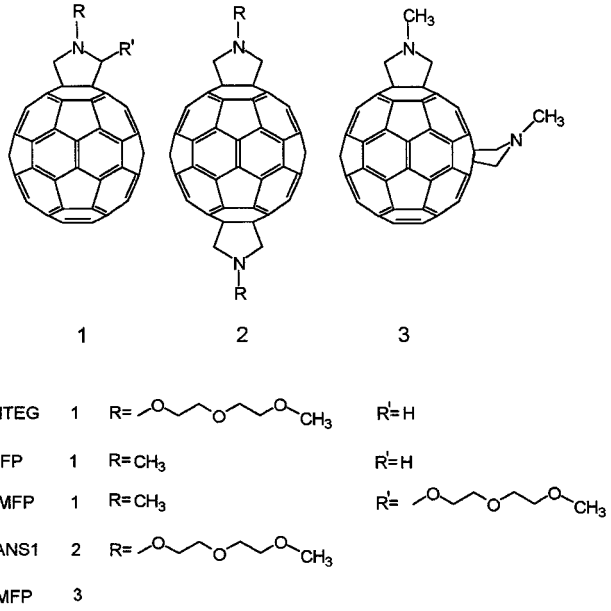

Experimental Section

Instrumentation. X-band EPR measurements were performed with a computer controlled Bruker ER 200 D spectrometer, equipped with a nitrogen flow-temperature controller. For *g* values calibration, the microwave frequency was measured with a 5342A Hewlett-Packard microwave frequency counter, and a LiTCNQ crystal was used as *g* value standard.

The pulsed EPR experiments were performed in the 110−300 K temperature range, using a Bruker ESP 380 spectrometer equipped with a dielectric Bruker cavity and a variable temperature unit.

The HF-EPR spectra (around 110 and 220 GHz) were obtained at the NHMFL in Tallahassee (FL) with a homemade spectrometer.[21] This machine is built around a superconducting magnet with a 17 T "main" coil and a ± 0.1 T "sweep" coil (Oxford Instruments Inc.). The source which has been used in this work is a Gunn oscillator emitting in the 108 to 112 GHz range, and equipped with a Schottky diode harmonic generator for obtaining higher frequencies (ABmm, Paris). The operating microwave frequency is measured with, and frequency locked to a source locking microwave counter (EIP 578B from EIP Microwave Inc., Milpitas, Ca).

The spectrometer was used in its basic configuration ("single pass" transmission mode), that uses oversized-cylindrical waveguides for propagation of the microwave power.

The transmission probe is in a liquid helium flow cryostat of the dynamic type (CF 1200 from Oxford Instruments Inc.); this ensures a good thermal exchange between the cold helium gas and the sample. The temperature is monitored within ± 0.1 degree. With a calibrated thermometer, Lakeshore model CX-1030-SD fixed a few millimeters to the side of the sample, the temperature we measured, in the 100 to 150 K range, was within ±2 deg of the temperature of the Oxford CF1200 sensor.

We used a liquid helium cooled In−Sb "hot electron" bolometer (QMC Instruments, London).

The spectra were obtained by modulation of the magnetic field at a frequency of 8 kHz with a modulation amplitude of 0.01−0.07 mT for spectra in liquid solution and of 0.1−0.15 mT for spectra in rigid phase. The main coil was in persistent mode and the magnetic field changed by variation of the additional field of the sweep coil. At 110 GHz, the spectra were recorded between 280 and 20 K for the $NTEG^-$ sample and between 185 and 80 K for the $TRANS1^-$ sample. At 220 GHz only spectra in the rigid phase limit ($T < 120$ K) were recorded. For *g* factor measurements DPPH (Sigma, ground to fine powder)[22] was used as internal standard to calibrate the magnetic field.

Materials. Functionalized fullerenes considered in this paper are shown in Scheme 1. The compounds are fulleropyrrolidine derivatives, prepared by reaction of the appropriate azomethine ylide precursor with C_{60}.[17] The synthesis of NTEG-fulleropyrrolidine (NTEG) has already been reported in the literature.[23] Compound TRANS1 is the trans1-bisadduct of the biscycloaddition of TEG-glycine and paraformaldehyde to C_{60}. This molecule was synthesized by the reaction of 2 equiv of TEG-glycine, 1 equiv of C_{60} and 10 equiv of paraformaldehyde in refluxing toluene, while the reaction was followed by HPLC. Then, it was purified by medium-pressure column chromatography and further purified by semipreparative HPLC column chromatography. The material was characterized by a variety of spectroscopic techniques, including ES-MS, ^{1}H and ^{13}C NMR, UV/vis, FT-IR and elemental analysis.[24]

Dibenzo-18-crown-6 was used as purchased from Aldrich. Methyltetrahydrofuran (mp 137 K) was distilled over sodium prior to use.

Abbreviations Used. MFP = *N*-methyl-3,4-fulleropyrrolidine (2′*H*-[5,6]fullereno-C_{60}-Ih-[1,9-c]pyrrole, 1′,5′-dihydro-1′-methyl-); tegMFP = *N*-methyl-2-(3,6,9-trioxadecyl)-3,4-fulleropyrrolidine (2′*H*-[5,6]fullereno-C_{60}-Ih-[1,9-c]pyrrole, 1′,5′-dihydro-1′-methyl-2′-[[2-(2-methoxyethoxy)ethoxy]methyl]); bisMFP = bis-[*N*-methyl-3,4-fulleropyrrolidine]; NTEG = *N*-(3,6,9-trioxadecyl)-3,4-fulleropyrrolidine (2′*H*-[5,6]fullereno-C_{60}-Ih-[1,9-c]pyrrole, 1′,5′-dihydro-1′-[2-[2-(2-methoxyethoxy)ethoxy]-ethyl]); TRANS1 = bis-TRANS1-[*N*-(3,6,9-trioxadecyl)-3,4-fulleropyrrolidine]; TEG = 3,6,9-trioxadecyl; THF = tetrahydrofuran; MeTHF = 2-methyltetrahydrofuran.

Anion Preparation. The radical anions of NTEG and TRANS1 were prepared by standard vacuum (10^{-4} mbar) techniques in a 10 mm o.d. Pyrex tube. The tube was equipped with three lateral arms. The first one contained the fullerene sample, in some cases together with the dibenzo-18-crown-6 ether. In the second one a sodium mirror was formed by evaporating the pure metal from a sodium-filled Drummond calibrated capillary, before introducing the solvent through the vacuum line. The third arm was equipped with an usual EPR tube.

The concentrations of the samples were 10^{-5} M.

Results

Continuous Wave (cw) X-Band EPR. The spectra at different temperatures for $NTEG^-$ and $TRANS1^-$ in liquid solution of MeTHF are reported in Figure 1. The spectra show the hyperfine structure due to the coupling with one nucleus of ^{14}N in the case of $NTEG^-$, and with two equivalent ^{14}N nuclei in the case of $TRANS1^-$. The hyperfine coupling constants (hcc's) are reported in Table 1. In the same table we report also the ^{14}N hcc's of other FP^- for comparison.

In Figure 2 the hyperfine structures of the satellite lines due to the radicals $NTEG^-$ and $TRANS1^-$ bearing a ^{13}C nucleus are shown, together with the simulated spectra.

The simulations were obtained on the basis of a best fit procedure on varying the number of different ^{13}C hyperfine couplings, the relative abundances of the radicals bearing each type of coupled ^{13}C nucleus, and the values of the hyperfine coupling constants. The results are reported in Table 2.

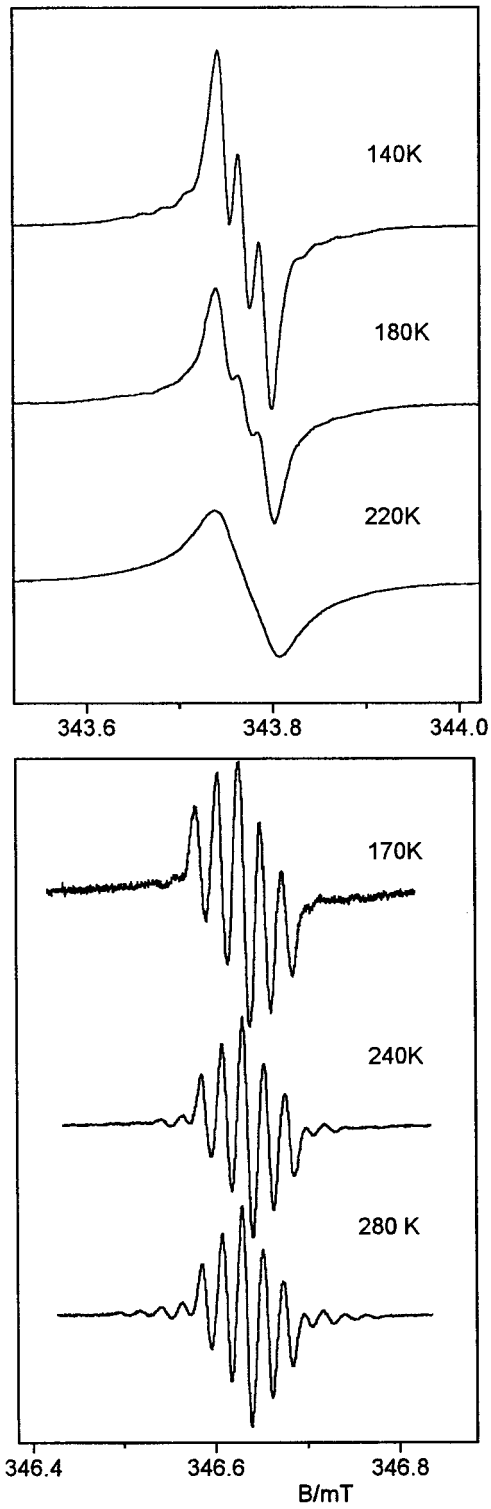

Figure 1. X-band EPR spectra of the radical anion NTEG$^-$ (upper spectra) and TRANS1$^-$ in MeTHF at different temperatures in liquid solution. The line widths vs the temperature are reported in Figure 3.

The EPR line shapes of NTEG$^-$ and TRANS1$^-$ depend in a different way on the temperature, as can be seen in Figure 1. The simulation of the spectra gives the peak-to-peak line width dependence on the temperature reported in Figure 3. One can see that the temperature dependence of the line widths has an opposite trend for the two compounds. In fact, on increasing the temperature the line width decreases for TRANS1$^-$ and increases for NTEG$^-$. The line widths for the two compounds become similar at low temperature. In the figure the contribution to the line width expected on the basis of the tumbling in MeTHF solution for both NTEG$^-$ and TRANS1$^-$ is also reported (see eqs 4 and 5 below).

TABLE 1: ^{14}N Hyperfine Coupling Constants for Some Fulleropyrrolidines Radical Anions (Values in mT)

^{14}N hcc	NTEG[b]	TRANS1[b]	MFP[a]	tegMFP[a]	bisNMP[a,c]
experimental	0.022	0.021	0.022	0.023	0.021 0.025
calculated	0.028	0.026			

[a] Reference 20. [b] This work. [c] Two radicals were observed.

Pulsed EPR. In liquid solution an FID was detected for both radicals. The agreement between the T_2 values obtained from the FID and that obtained from the cw-EPR line widths has been checked for some temperatures. To get the T_1 values in liquid solution, we performed an inversion recovery of the magnetization. This was observed with the pulse sequence $\pi-T-\pi/2-t$ by varying the time T between the inverting pulse and the $\pi/2$ pulse giving rise to the FID. The lengths of the π and $\pi/2$ pulses were 24 and 16 ns, respectively. A monoexponential fit of the recovery curve gave the T_1 values at the different temperatures.

We find $T_1 = 2800$ ns for TRANS1$^-$ at room temperature, and in liquid solution the value increases slightly on decreasing the temperature. A much shorter T_1 was measured for NTEG$^-$, and the value is strongly temperature dependent. The logarithmic plot of $1/T_1$ values of NTEG$^-$ versus $1/T$ is reported in Figure 4.

High-Frequency EPR. The 110 GHz EPR spectra of NTEG$^-$ in MeTHF liquid solution show a single line without any hyperfine structure. The line width slightly decreases from room temperature to 230 K ($\Delta B_{pp} = 0.06$ mT), then it increases up to 0.25 mT at 160 K and 0.39 mT at 150 K. The spectra in the range 100−150 K are reported in Figure 5, upper spectrum.

At 130 K a slow motion spectrum appears showing **g** tensor anisotropy. The spectrum changes on further decreasing the temperature. The lines sharpen slightly and the splitting between the features corresponding to the **g** tensor components increases (see Figure 5). At 100 K a spectrum is obtained that does not change on further lowering the temperature. Below 100 K the spectrum has been recorded using a very low microwave power, to avoid fast passage effects.

EPR spectra of TRANS1$^-$ have been recorded at 110 GHz up to 185 K. At this temperature the spectrum consists of a single line with $\Delta B_{pp} = 0.27$ mT.

On lowering the temperature, at 130 K a powder spectrum appears showing anisotropy due to a quasi-axial **g** tensor. On further decreasing of the temperature the spectrum changes only slightly (see Figure 5).

The **g** tensor components of both radicals have been determined by simulating spectra taken at about 220 GHz. At the magnetic fields of interest, the calibration of the magnet and the linearity of the sweeps were tested using DPPH and Mn^{2+} centers in a polycrystalline MnO/CaO standard.[21,25] For the experimental spectra we report in this paper we only use DPPH for calibration. For this work, the accuracy of the field measurement was $\pm 1.25 \times 10^{-5}$.

The experimental spectra with simulations are reported in Figure 6 vs the g values. All the spectra have been corrected for the component due to the dispersion using a Hilbert transformation and then simulated using the Symphonia program from Bruker, with Lorentzian line shapes. The line width parameters are reported in the caption of Figure 6. The **g** tensors are reported in Table 3.

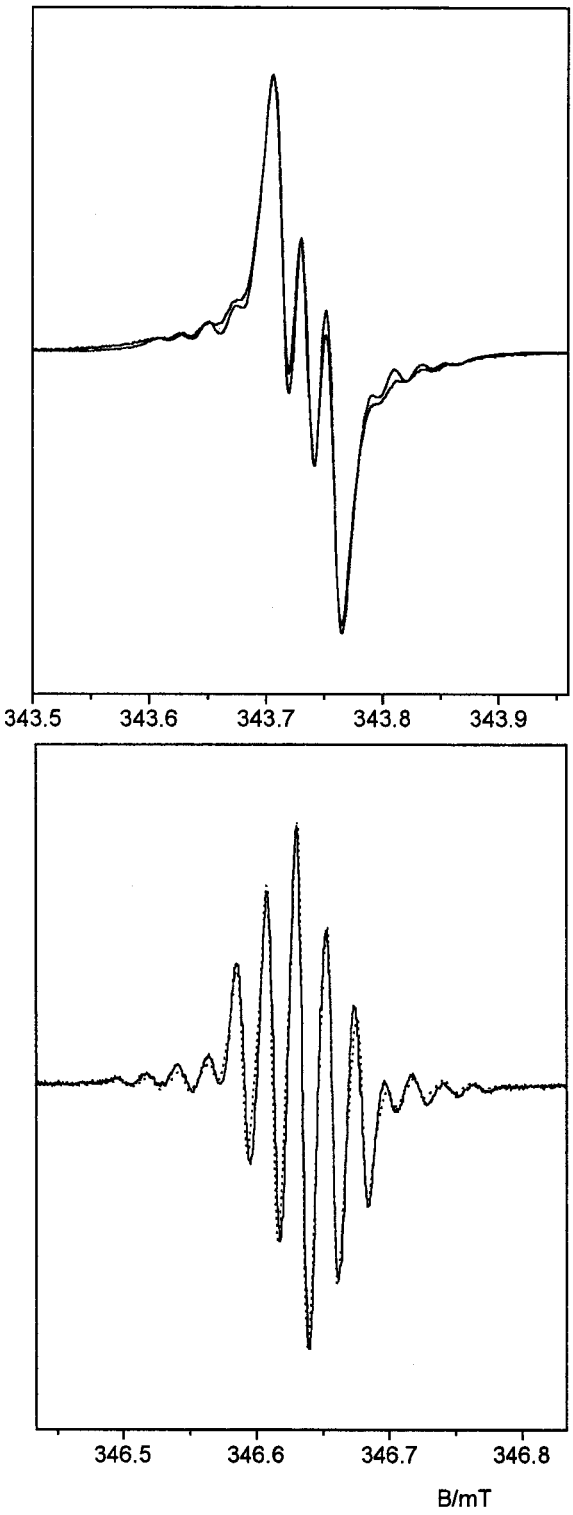

Figure 2. Experimental (continuous line) and simulated X-band spectra of $NTEG^-$ (upper spectrum, $T = 160$ K) and $TRANS1^-$ ($T = 280$ K) in MeTHF solution, showing the satellite lines due to radical anions bearing a ^{13}C nucleus. For the parameters of the simulation see Table 2.

Calculations

Semiempirical and ab initio quantum chemical calculations were performed for the mono- and trans bis-pyrrolidine-adducts of fullerene and for their radical anions, by means of the packages GAUSSIAN 98,[26] MOPAC 93[27] and with the PC-GAMESS version[28] of the GAMESS (US) QC package.[29] The calculations were performed on pyrrolidine adducts where simpler *N*-methyl groups substituted the *N*-polyalkoxy chains. Geometry optimizations carried out by using the semiempirical PM3 Hamiltonian on both neutral molecules provided the most stable structures with the pyrrolidine ring in its envelope conformation (but the flap angle of 24° was smaller than the experimental one[30]) and an axial position for the *N*-methyl group. However, a different conformation, with an equatorial *N*-methyl group, was also found, with only 0.5 kcal/mol energy difference. This latter conformation, with the nitrogen lone pair pointing toward the π orbitals of the fullerene ball (Figure 7), was used in the subsequent calculations. As a matter of fact, geometry optimization at the ab initio (STO-3G) level gives, as the most stable equilibrium structure, an envelope-CH_3-equatorial conformation for the pyrrolidine ring, with a more correct 36° flap angle.[30]

Semiempirical single point electronic energy calculations, at the neutral molecule (semiempirical) geometry, were carried out for the anion radicals, to get an estimate of the spin density distribution. Unrestricted open shell Hartree−Fock calculations, UHF,[31] that would have easily allowed for the contribution of spin-polarization, gave unreliable results owing to the strong spin contamination of the doublet by higher spin states ($\langle S^2 \rangle = 4.684$). We tried two types of restricted semiempirical HF calculations: the correct restricted open shell (ROHF),[32] with PC-GAMESS, and the half-electron approximation (RHF-HE)[33]

TABLE 2: ^{13}C Hyperfine Coupling Constants and Number of Equivalent Positions for each hcc of NTEG and TRANS1 Radical Anions (Values in mT)

NTEG	*n* equivalent ^{13}C	2	2	4	4
	A (^{13}C)	0.200	0.165	0.112	0.070
TRANS1	*n* equivalent ^{13}C	4	8		
	A (^{13}C)	0.176	0.046		

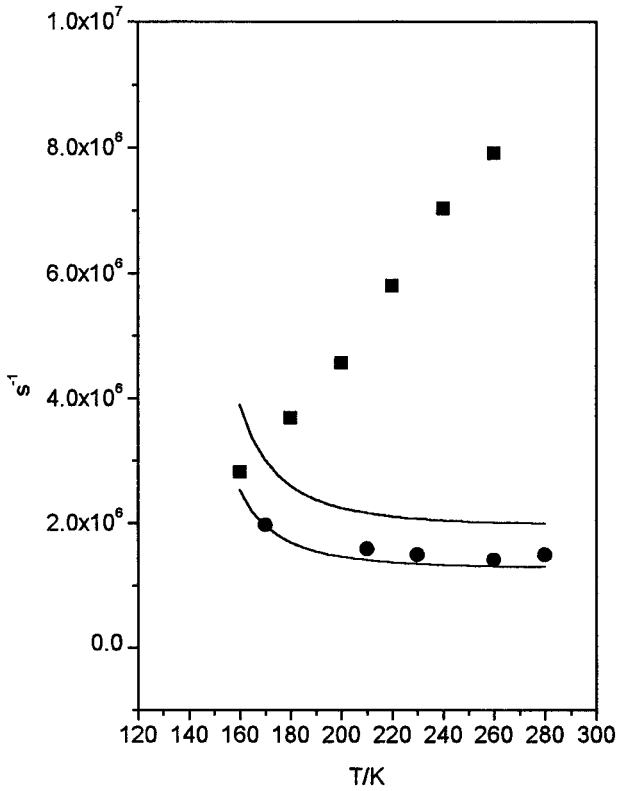

Figure 3. Temperature dependence of the X-band EPR peak-to-peak line widths of $NTEG^-$ (squares) and $TRANS1^-$ (circles). The lines show the calculated contribution to the line widths due to the modulation of the spin Hamiltonian parameters by the reorientation in solution (see text). Key: lower line, $TRANS1^-$; upper line, $NTEG^-$.

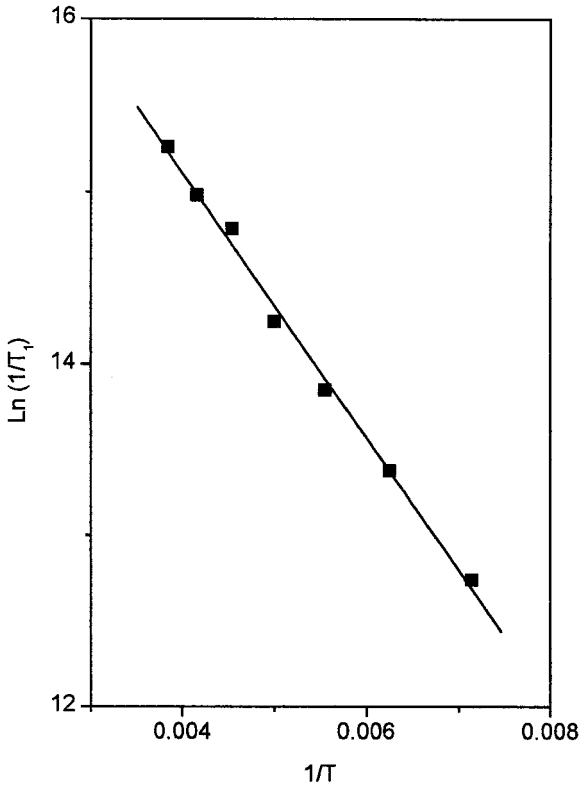

Figure 4. Logarithmic plot of $1/T_1$ (s^{-1}) vs $1/T$ for $NTEG^-$. The electron spin−lattice relaxation time T_1 is obtained by pulsed EPR spectroscopy following the inversion recovery of the magnetization.

using Gaussian and MOPAC93 packages. Since the first method provides results not consistent with the molecular symmetry only the results obtained using the RHF-HE method will be reported.

To compare the spin density distribution with the experimental ^{13}C hcc's', the values of the computed semiempirical total atomic spin density of the 2s orbital component are shown in Tables 4 and 5 for the 12 carbon atoms with the highest spin densities. In the same tables are reported also the ^{13}C hcc's' obtained with the expression:

$$a(^{13}C) = 134.77\rho^{C}_{2s} \quad (1)$$

where 134.77 mT is the ^{13}C hcc for one electron in a 2s orbital.[34]

The spin density distribution is also shown in Figure 8 with different intensities of the colored balls. The data show that the unpaired electron is mainly localized on the fullerene belt and its distribution corresponds to the molecular symmetry (C_s for the monoadduct and C_{2h} for the bisadduct).

UHF single point calculations, at the ab initio (STO-3G) optimized neutral molecule geometries, were also performed with the density functional method, as implemented in GAUSSIAN98. The Becke's three Parameter hybrid exchange Functional[35] as modified by the LYP correlation functional[36] (B3LYP) was used in the calculations, with a 6-31G(d) basis set. In this case the ^{13}C and ^{14}N hcc's' can be obtained directly, and their values are reported respectively in Tables 4 and 5, and in Table 1.

Even with this more sophisticated method, which is reported to be very effective in reproducing the effects of spin polarization with minimal spin contamination (we obtained a very good value of $\langle S^2 \rangle = 0.755$), the ^{13}C hcc's' distribution is very similar to that obtained with semiempirical RHF methods and with a worse geometrical structure. The hcc's' are higher than the previous ones and with only small differences between them.

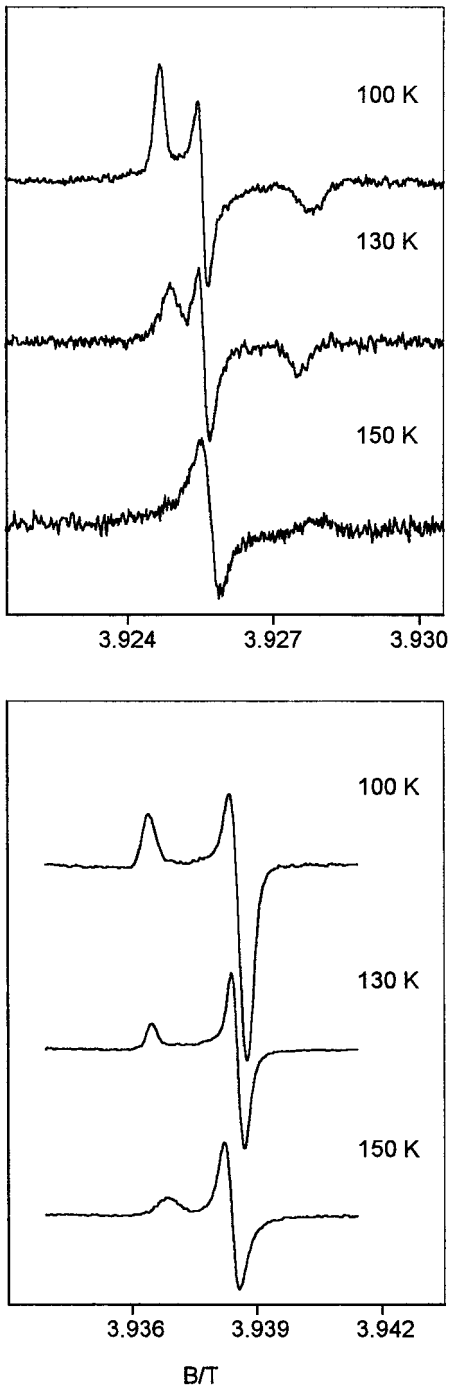

Figure 5. W-band EPR spectra of $NTEG^-$ (upper spectrum) and $TRANS1^-$ in liquid solution of MeTHF near to the freezing point of the solvent and in frozen solutions.

Discussion

HF-EPR Spectra, g Tensors and *g* Factors. The *g* factors of fullerene anion radicals in solution are typically shifted to unusually low values if compared with the free electron: the C_{60} monoanion *g* factor is shifted to around 2.0000. The actual value changes slightly with the solvent and the counterion.[5,16,37,43]

As known, the *g* factor depends on the electronic state of the radical, and on the spin−orbit coupling constants of the atoms in the radical. A highly symmetric electron distribution is expected to affect the *g* factors because of a more efficient spin−orbit mixing due to the quasi degenerate excited electronic states. Moreover, it has been stressed[37] that the calculation of the *g*

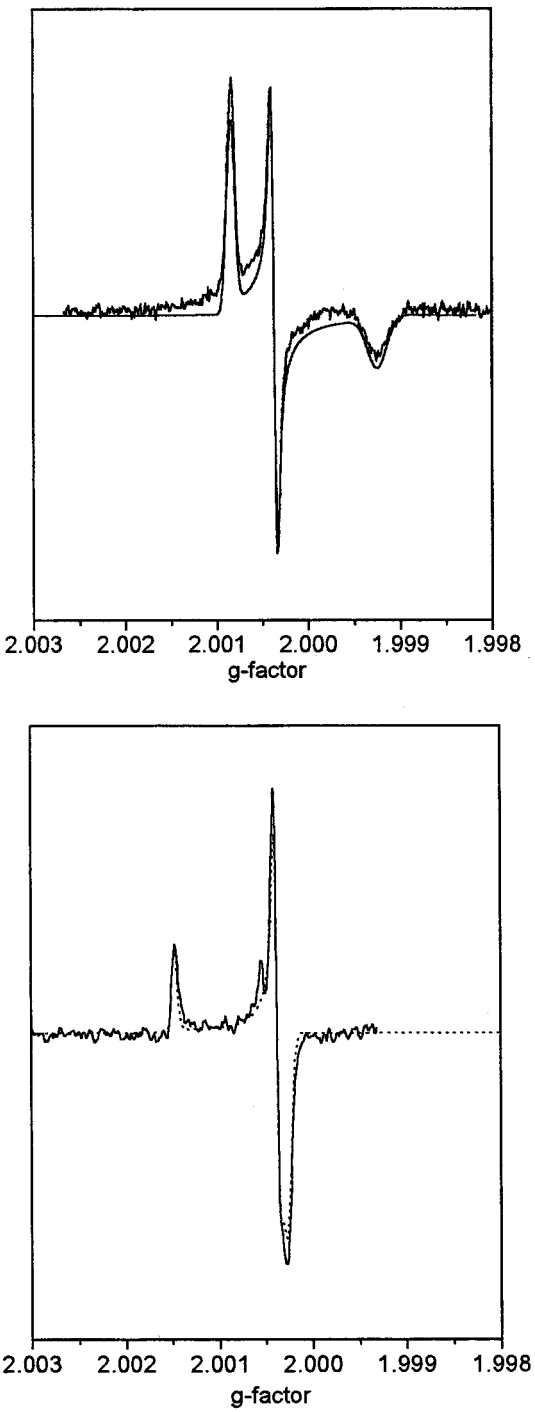

Figure 6. Experimental and simulated HF-EPR spectra of $NTEG^-$ (upper spectrum) and $TRANS1^-$ in rigid matrix of MeTHF ($\nu = 220$ GHz). The parameters for the simulations are the following. $NTEG^-$: $g_{xx} = 2.00085$, $g_{yy} = 2.00038$, $g_{zz} = 1.99925$; inhomogeneous line widths for the three components, respectively, 0.28 mT, 0.20 mT and 0.68 mT; $TRANS1^-$, $g_{xx} = 2.00147$, $g_{yy} = 2.00038$, $g_{zz} = 2.00027$; inhomogeneous line width for the three components, 0.21 mT.

factor for the C_{60} monoanion should take into account the possible dynamic Jahn−Teller effect, and the coupling between electronic and vibrational states.

Several theoretical calculations of the g factors for the C_{60} radical monoanions can be found in the literature,[38] but a satisfactory agreement between calculations and experimental values is still lacking.

In Table 6 we report the g factors of some FP radical anions. One can see that the g factors of the monoadducts FP radical anions are very similar to those of the parent compound, and therefore the electronic properties of the former radicals cannot be very different from those of the latter one.

On the other hand, the g factors of bisadducts FP radical anions are shifted toward a larger value, closer to that of the free electron. On the basis of the previous considerations, this

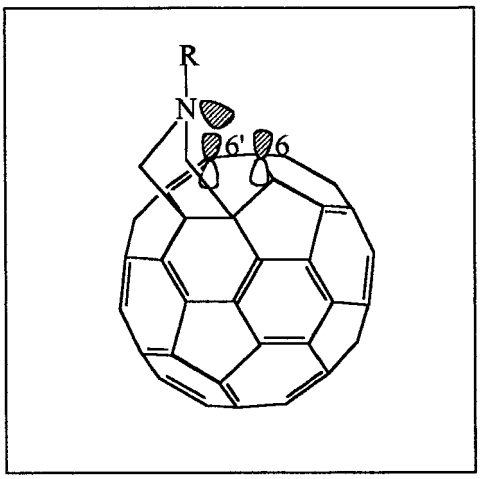

Figure 7. Conformation of the pyrrolidine ring with the R group in axial position, allowing a mixing between the N lone pair and the 2p orbitals on carbon atoms 6 and 6′.

TABLE 3: g Tensors Obtained from HF-EPR Spectra in Glassy Solutions of MeTHF[a]

	g_x	g_y	g_z	$\langle g \rangle$
NTEG	2.00085	2.00038	1.99925	2.00016
TRANS1	2.00147	2.00038	2.00027	2.00071

[a] In the last column the average g value is reported.

TABLE 4: Total Atomic Spin Density of the 2s Orbital for the Carbon Nuclei of $NTEG^-$ and Calculated ^{13}C hcc's

carbon atom[a]	ρ_{2s}[b]	^{13}C hcc[c]	^{13}C hcc[d]
12, 12′	0.001257	0.17	0.31
9, 9′	0.001138	0.15	0.27
27	0.00108	0.14	0.30
16	0.000954	0.13	0.26
26	0.000925	0.12	0.21
17	0.000874	0.12	0.24
20, 20′	0.000825	0.11	0.25
23, 23′	0.000776	0.10	0.22

[a] For the numbering of the atoms see Figure 8. [b] 2s spin densities calculated by PM3/RHF−HE method. [c] ^{13}C hyperfine coupling constants (mT) calculated by relationship (1) and the 2s spin densities obtained by PM3/RHF−HE method. [d] ^{13}C hyperfine coupling constants (mT) calculated by the density functional method.

TABLE 5: Total Atomic Spin Density of the 2s Orbital for the Carbon Nuclei of $TRANS1^-$ and Calculated ^{13}C hcc's.

carbon atom[a]	ρ_{2s}[b]	^{13}C hcc[c]	^{13}C hcc[d]
20, 20′			
12, 12′	0.001102	0.15	0.29
9, 9′			
23, 23′	0.000989	0.13	0.25
17	0.000975		
27	0.000973	0.13	0.28
16	0.000941		
26	0.000939	0.13	0.25

[a] For the numbering of the atoms see Figure 8. [b] 2s spin densities calculated by PM3/RHF−HE method. [c] ^{13}C hyperfine coupling constants (mT) calculated by relationship (1) and the 2s spin densities obtained by PM3/RHF−HE method. [d] ^{13}C hyperfine coupling constants (mT) calculated by the density functional method.

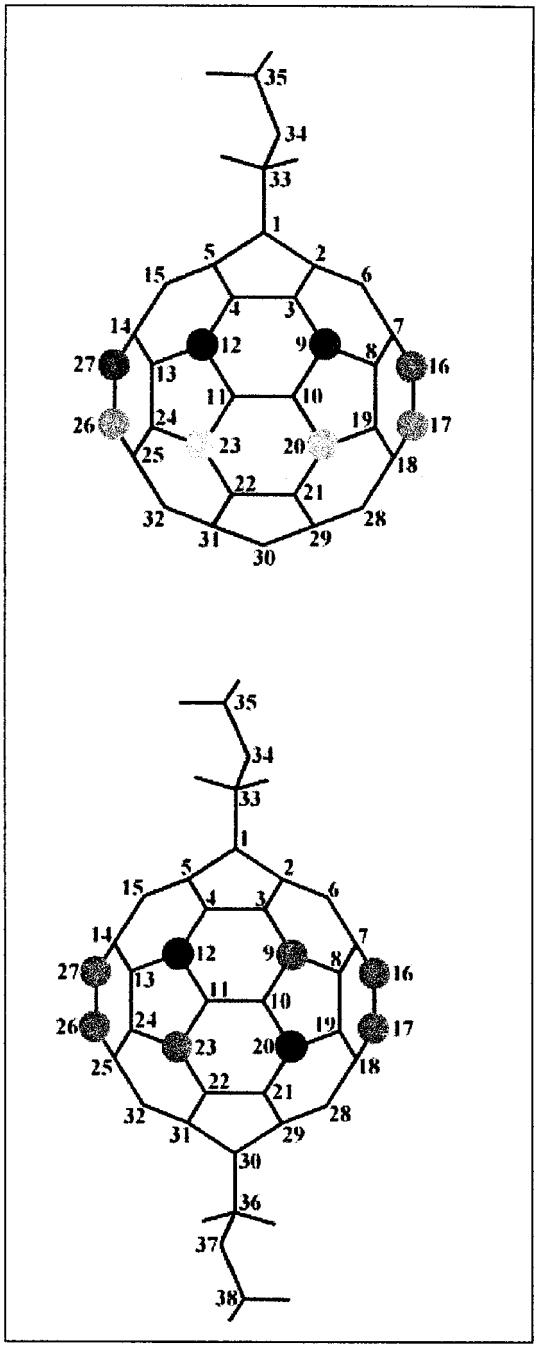

Figure 8. Numbering of the carbon atoms for the two compounds NTEG and TRANS1. The molecular structure is laying on a symmetry plane, the atom C′ below the plane corresponding to atom C above. The positions with a circle correspond to the 12 carbon atoms bearing the highest spin densities on the 2s orbital. The intensity of the gray indicates the spin density level, see Tables 4 and 5.

effect could be attributed to a lower symmetry of the electron distribution, or to a different structural rigidity of the fullerene sphere.

On the basis of the experimental results the electron distribution in the bisadduct TRANS1$^-$ is found to have a higher symmetry with respect to the monoadduct NTEG$^-$. Therefore, we can suppose that the low value of the *g* factors of fullerene anions could originate in the low structural rigidity of these compounds.

In the case of TRANS1 and of the other bisadducts, we can expect that the presence of two pairs of carbon atoms with a sp^3 hybridization can give rise to a stiffer structure, and as a consequence the *g* factor of the bisadducts is more similar to that of the free electron.

TABLE 6: *g* Factors for Radical Anions of C_{60} and Some FP Derivatives in Liquid Solution[a]

	g factor	ref.
C_{60}	2.0000	15
MFP (MeTHF)	1.9999	20
TegMFP (MeTHF)	1.9999	20
BisMFP[b] (230 K) (MeTHF)	2.0013	20
	2.0011	
NTEG (MeTHF)	1.9999	this work
TRANS1 (MeTHF)	2.0003	this work

[a] The error is ±0.0002. [b] Two radicals were observed.

A different rigidity of NTEG and TRANS1 can be inferred also from the low-temperature HF-EPR spectra of the two radical anions. As can be seen in Figure 5, the spectra of the two radicals show a different behavior in the frozen MeTHF matrix in the range 100−130 K. In the spectrum of NTEG$^-$ the EPR lines are moving apart on decreasing the temperature, and the spectrum at 130 K still shows slow motion effects, whereas TRANS1$^-$ at this temperature gives a more rigid matrix spectrum. Moreover, the spectrum of NTEG$^-$ in Figure 6, recorded at a frequency near to 220 GHz, was simulated with three different inhomogeneous line widths for the three components (respectively, 0.28, 0.2 and 0.68 mT for the g_{xx}, g_{yy} and g_{zz} components), whereas the simulation for TRANS1$^-$ was done with about the same line width for the three components (0.21 mT). The different inhomogeneous broadening, with a larger broadening for one of the components in the NTEG$^-$ spectrum, suggests for this latter radical the presence of more conformations slightly distorted along one of the principal axes of the **g** tensor. To confirm this conclusion we compared the EPR spectra of NTEG$^-$ taken at 220 and 110 GHz, and found a substantial dependence of the line widths on the frequency. In fact, the spectrum at 110 GHz is simulated with respectively, 0.17, 0.13 and 0.38 mT for the g_{xx}, g_{yy} and g_{zz} components.

^{14}N Hyperfine Couplings. In Table 1 we report the ^{14}N hyperfine couplings for radical anions of some fulleropyrrolidine mono- and bisadducts. It is worth to be noted that for all the reported radicals the ^{14}N hyperfine couplings are very similar, independently of their being mono- or bisadducts, and for the latter ones independently of their symmetry.

The values of the ^{14}N hyperfine couplings for NTEG$^-$ and TRANS1$^-$ calculated with the density functional method are also reported in Table 1. The agreement with the experimental values is very good. In ref 20 we discussed the origin of the ^{14}N hyperfine coupling, and we concluded that it is too large to be explained by a spin polarization of the C−C and C−N bonds. The spin density must derive therefore from a direct transfer from the π distribution on the bucky ball to the sp^3 lone pair orbital of the nitrogen atom, in agreement with the mechanism of periconjugation.[39] The lone pair of the nitrogen in the bent pyrrolidine ring is overlapping with the p orbitals on carbon atoms 6 and 6′ (see Figures 7 and 8). Therefore, the value of the ^{14}N hyperfine coupling, assuming that the conformation of the pyrrolidine ring does not vary for the different adducts, is a direct measure of the spin density distribution on the two carbon atoms interacting with the nitrogen lone pair. As a consequence we must conclude that the spin density near the pyrrolidine rings is the same for all the adducts, and it is determined by a local symmetry of the spin distribution due to the periconjugation with the nitrogen lone pair and not to the symmetry of the whole π distribution on the bucky ball.

^{13}C Hyperfine Couplings. The experimental ^{13}C hyperfine couplings reported in Table 2 involve in both TRANS1$^-$ and NTEG$^-$ 12 carbon atoms, grouped in four sets of equivalent hcc's in the case of NTEG$^-$, and in two sets in the case of TRANS1$^-$. This confirms that the symmetry of spin distribution in TRANS1$^-$ is higher than in NTEG$^-$.

The calculated hcc's data do not show any clear correspondence with experimental ones as regard their grouping in equivalent nuclei sets, the calculated spin distribution being more homogeneous, with all the hcc's very similar between them. Moreover the hcc's calculated by the density functional method are all bigger than the experimental ones.

The only correspondence between experimental and calculated spin density distribution is its heaping up on 12 carbon atoms. According to the calculations they are the carbon atoms in the equatorial belt of the radicals, shown in Figure 8.

It should be noted that the ^{13}C hcc's depend strongly on the partial s character of the orbital bearing the unpaired electron. This depends in turn on the geometry of the radical anion that has been optimized for the neutral molecule and not for the radical.

It is worth to compare the ^{13}C hyperfine couplings for the radical anion of TRANS1 with those of another trans1-fullerene bisadduct, reported by Brezová et al.[40] For the anion radical of $C_{60}(C(COOEt)_2)_2$ the authors find three groups of 4 equivalent nuclei ^{13}C, corresponding to hcc's of 0.19, 0.0854, and 0.0684 mT. There is a substantial agreement of their results with the data reported in Table 2, both for the number of ^{13}C showing a hcc of this order of magnitude (12 in both cases), and also for the values of the hcc's. In the quoted paper, the authors assume that the spin density is mainly located on the keto groups, and therefore they attribute the largest splitting constant to the ^{13}C in the latter groups.

On the basis of the experimental results and of the spin density calculations reported above, we conclude instead as most probable that also for the C_{60} derivatives in ref 40 the ^{13}C hcc's. are due to the fullerene carbon atoms of the equatorial belt, with a spin density distribution similar to that reported in Figure 8. In fact the π electron distribution on the fullerene moiety of a trans1-C_{60} bisadduct should not be substantially modified by the different attached groups, as long as a π conjugation with these latter is not present.

cw-EPR Line Widths and T_1 Values. In general the EPR line widths of radicals in dilute solutions depend mainly on the modulation of the Zeeman and hyperfine interactions due to the rotational diffusion. For rotational correlation times typical of medium-sized radicals in low viscosity solutions, only the secular and pseudosecular contributions to the electron spin relaxation must be taken into account in the X-band EPR spectroscopy. Therefore, in this motion régime the spin−lattice time T_1 is longer than the spin−spin relaxation time T_2. The line widths are proportional to the correlation time of the motion, and they increase on increasing the viscosity of the solution.

In the Redfield approximation[34] the line width contribution due to the tumbling in solution is proportional to η/T, where η is the viscosity. The viscosity for MeTHF[41] was obtained by the relationship

$$\log_{10}\eta = -3.986 + 162/(T - 81) \qquad (2)$$

($[\eta]$ = kg m^{-1} s^{-1}).

For TRANS1$^-$ at $T = 170$ K the experimental peak-to-peak line width is $\Delta B_{pp} = 2 \times 10^6$ s^{-1}.

By considering a fixed contribution to the cw-EPR line width due to the 100 kHz modulation sidebands (200 kHz → 1.25×10^6 s^{-1}), we obtain a contribution due to the tumbling in solution: $(\Delta B_{pp})_{tumb} = 7.5 \times 10^5$ s^{-1}, corresponding to a spin−spin relaxation rate

$$\left(\frac{1}{T_2}\right)_{tumb} = \frac{\sqrt{3}}{2}(\Delta B_{pp})_{tumb} = 6.5 \times 10^5 \text{ s}^{-1} \qquad (3)$$

By taking into account the proportionality of $1/T_2$ to η/T, and by using eq 2, we obtain the temperature dependence of the line width reported in Figure 3 as a continuous line. The agreement with the experimental values indicates that the temperature dependence of the line width for this radical is determined by its tumbling in solution.

It should be noted that, despite the relatively bulky radical, the line widths are small. This is due to the small anisotropies of the hyperfine and **g** tensors of the radicals.

In fact, in the Redfield limit the line width contribution due to the tumbling for an electron spin coupled with a nucleus with spin quantum number M_I is given by[34]

$$\left(\frac{1}{T_2}\right)_{tumb} = A + BM_1 + CM_1^2 \qquad (4)$$

The three coefficients are

$$A = \frac{2}{15}\left(\frac{\mu_B B_z}{\hbar}\right)^2 (g^0{:}g^0)\tau_c$$

$$B = \frac{4}{15}\left(\frac{\mu_B B_z}{\hbar}\right)(g^0{:}T_N^0)\tau_c$$

$$C = \frac{2}{15}\frac{1}{\hbar^2}(T_N^0{:}T_N^0)\tau_c \qquad (5)$$

where in the inner products g^0 and T_N^0 are, respectively, the deviations of the **g** tensor and of the hyperfine tensor $\mathbf{T_N}$ from the average values, and τ_c is the correlation time of the tumbling motion. In the Debye approximation:

$$\tau_c = \frac{4\pi\eta r_0^3}{3k_B T} \qquad (6)$$

where η is the viscosity of the solution and r_0 is the radius of the radical.

For the radicals of NTEG and TRANS1, due to the small value of the ^{14}N hcc, and therefore of the corresponding hyperfine tensor, the largest contribution is expected to be due to the A parameter in (5). From the principal values of the **g** tensors of the two radicals measured by HF-EPR (see Table 3), the $(g^0{:}g^0)$ value can be obtained: 1.35×10^{-6} for NTEG$^-$, 8.8×10^{-7} for TRANS1$^-$.

For $B = 330$ mT, we obtain for the A parameter in eqs 5 the values $A/\text{s}^{-1} = 1.5 \times 10^{14}\tau_c$ for NTEG$^-$, and $A/\text{s}^{-1} = 9.9 \times 10^{13}\tau_c$ for TRANS1$^-$.

By comparing the experimental value for $1/T_2$ at 170 K obtained above, and by using eqs 5 and 6, we estimate the radius of TRANS1$^-$. A value of $\tau_c = 6.6 \times 10^{-9}$ s, is obtained, giving $2r_0 \approx 8$ Å, in good agreement with the expected average radius for the radical.

The line width contribution due to the tumbling for NTEG$^-$ can be obtained from that of TRANS1$^-$; the former is expected to be 1.5 times that of the latter (see the upper line in Figure 3), on the basis of the values of the A parameters reported above.

TABLE 7: Activation Energies from the Arrhenius Plot of the EPR Line Widths

	Δ/hc, cm^{-1}	ref
C_{60}^- (THF−pyridine, glassy solution)	240	42
MFP^- (MeTHF, liquid solution)	652	20
$NTEG^-$ (MeTHF, liquid solution)	536	this work

The experimental temperature dependence of the line width of $NTEG^-$, also reported in Figure 3, cannot therefore be explained by the time modulation of the magnetic interactions due to the tumbling in solution. The line width increases on increasing the temperature. This result is similar to that obtained for the radical anion C_{60}^- (see ref 16 and references therein, and also refs 42 and 43) and the radical anions of other fulleropyrrolidines.[20] For these systems, it has been shown that the anomalous line widths were due to a non secular contribution. In fact, the electron spin−lattice relaxation times have been measured in these previous cases, and they have been found to be anomalously short.

For C_{60}^- the EPR line width at room temperature varies between 1 and 8 mT depending on the solvent and the counterion. In ref 42 by measuring the spin−lattice relaxation time T_1 it has been shown that the EPR line widths above 50 K are completely determined by the fast relaxation. The extrapolation of the T_1 values to higher temperatures gives a spin lifetime of $\approx$1 ns at room temperature.

In ref 20 we have shown that for the monoadducts fulleropyrrolidine radicals a similar effect is present, although much less pronounced, and we obtained a value $T_1 = 100$ ns at room temperature. However for the fulleropyrrolidine bisadducts much longer T_1 values were found.

In the present work, as reported above, we find a value $T_1 =$ 200 ns for $NTEG^-$ and $T_1 = 2800$ ns for $TRANS1^-$ at room temperature. Therefore, for the former radical we have a short T_1, similar to that of other fullerene pyrrolidine monoadducts, whereas the T_1 of $TRANS1^-$ is more than 10 times longer, as for other pyrrolidine bisadducts. The short T_1 of $NTEG^-$ means that there is a non secular contribution to the EPR line width similar to that already found for other C_{60} derivatives. This gives rise to the temperature dependence of the EPR line width in Figure 3. In Figure 4 we report the plot of $\ln(1/T_1)$ vs $1/T$ for the latter radical. The linear plot shows that a temperature activated process affects the lifetime of the spin state, with an activation energy $\Delta = 6.4 \pm 0.5$ kJ/mol (536 cm^{-1}). This activation energy can be compared with those measured for C_{60}^- and MFP^-. The values are reported in Table 7. It should be noted that for C_{60}^- the activation energy is obtained from the EPR line widths in glassy solution of THF−Pyridine; the line width varies smoothly through the temperature of the softening of the glass, suggesting that the tumbling of C_{60}^- is not affected significantly on going from glass to solution.[43] Different values of the activation energies, but of the same order of magnitude, are obtained in different solvents.[42,43] One can see that the values relative to the fulleropyrrolidine derivatives are of the same order of magnitude with respect to that of C_{60}^-.

Similar anomalous temperature dependence of the electron spin relaxation rate, increasing with the temperature, have been attributed in the past to spin-rotational relaxation mechanisms.[34] These effects are known to derive from a coupling between the electron spin magnetic moment and the magnetic moment of the rotating radical modulated in time by the interaction of the radical with the solvent. On increasing the viscosity of the solvent, the lifetime of the rotational angular momentum decreases, with a temperature dependence opposite with respect to that of the correlation time of the tumbling. A relation of

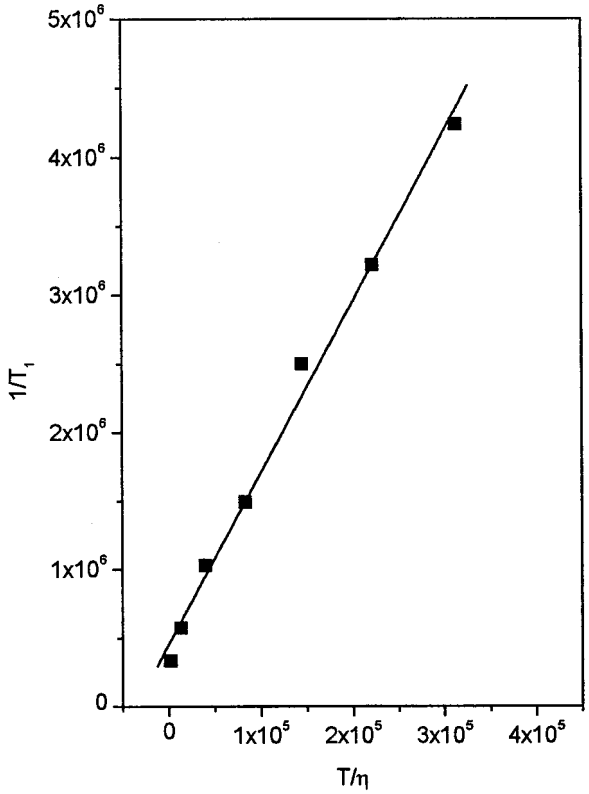

Figure 9. Plot of $1/T_1$ (s^{-1}) vs T/η for $NTEG^-$, where η is the viscosity of MeTHF (see text).

inverse proportionality between the reorientational correlation time τ_c and the correlation time of the angular momentum τ_J has been given by Hubbard.[44]

Therefore, the signature of the spin-rotational contribution is its linear dependence on the parameter T/η.

In Figure 9 we report the dependence of $(1/T_1)$ on T/η for $NTEG^-$ in MeTHF. As one can see, the linear dependence is quite good, pointing to a spin-rotational effect.

Spin rotational effects have been observed in the past for small size radicals and low viscosity solutions.[34] The spin Hamiltonian responsible for these effects is given by

$$H_{\text{spinrot}} = \mathbf{J}\cdot\tilde{\mathbf{C}}\cdot\mathbf{S} \tag{7}$$

where **J** is a magnetic moment due to the rotation of the slightly unbalanced charge distribution on the molecule, **S** is the electron spin magnetic moment and **C** is the spin-rotation coupling tensor. To apply the theory quantitatively, **C** must be known.

A simple expression for **C** and therefore for the spin rotational contribution to the line width can be obtained under the assumptions that **C** is time independent, that the molecule is rotating as a rigid rotor, and that a good model for the rotational diffusion is the Brownian motion. With these assumptions the relationship holds:

$$\left(\frac{1}{T_1}\right)_{sc} = \left(\frac{1}{T_2}\right)_{sr} = \frac{1}{9}\frac{\Delta\mathbf{g}:\Delta\mathbf{g}}{\tau_c} \tag{8}$$

where $\Delta\mathbf{g}$ is a tensor describing the deviation of **g** from the free spin value.[34]

By calculating from eq 6 the τ_c value for NTEG (with $2r_0 =$ 8 Å as for $TRANS1^-$, and obtaining $\Delta\mathbf{g}$ from the values in Table 3), we find at $T = 250$ K a contribution to the line width $(1/T_1)_{sr} = 10^3$ s^{-1}, which is 3 orders of magnitude smaller than the EPR line widths.

A similar calculation of the spin-rotational contribution to the line width of C_{60}^- has been done by Eaton at al., and they conclude that the calculated contribution is too small to be taken into account in determining the relaxation rate.[43]

However, the model used to obtain eq 8 is hardly acceptable for NTEG and C_{60}. In particular, the hypothesis of a rigid rotor seems unrealistic. Therefore, we cannot drop out the possibility of larger values of the coupling tensor **C** for these non rigid radicals. This assumption would be consistent with the larger spin-rotational effect on C_{60}, less rigid than NTEG, and also with the negligible effect on TRANS1, more rigid than NTEG as discussed above.

However, there is also another possible hypothesis on the origin of the observed line width effects. Apart the magnetic moment deriving from the rotation of the molecule, another possible spin-rotational contribution was foreseen by Kivelson and Atkins.[45] This is the contribution due to the spin−orbit interaction

$$H_{IS}(t) = \lambda l(t)\cdot\mathbf{S} \qquad (9)$$

time modulated by time fluctuations of the orbital angular momentum *l*.

It is well-known that for fullerene derivatives the near degeneracies of the electronic states allow radiationless transitions between the ground state and the low energy excited ones driven by the coupling with the solvent cage. This effect can be considered as producing an electron circulation on the fullerene π network, giving rise to an electron orbital angular momentum different from zero. In general the effect of spin Hamiltonian (9) for radicals is negligible, since the excited states are far away from the energy of the phonons of the solvent cage. As pointed out by Kivelson and Atkins this effect can become important for radicals with low lying excited states.

The efficiency of the relaxation mechanism in (9) depends on the lifetime of the orbital angular momentum *l*. As for the rotational angular momentum, its lifetime will decrease on increasing the viscosity of the solvent. Therefore, the relaxation rates for the time modulation of the orbital angular momentum should increase on increasing T/η, as for the spin-rotational relaxation.

We conclude that a spin-rotational relaxation mechanism, thermally activated with the energies listed in Table 7, is responsible for the anomalous temperature dependence of the EPR line widths of the fullerene radical anions.

Conclusions

The spin Hamiltonian parameters of the monoadduct and the bisadduct fulleropyrrolidine radical anions studied in this paper have been fully characterized. In particular, for the first time full **g** tensors for two fulleropyrrolidine radical anions have been determined, by means of high-frequency EPR spectra at low temperature.

Some features were already observed in a previous work for similar adducts,[20] and have been confirmed in the present one. Among them, the origin of the ^{14}N hyperfine couplings due to the bending of the pyrrolidine ring that allows a direct mixing of the lone pair orbital on the nitrogen atom with the π distribution on the fullerene. In this paper calculations performed with the density functional method have given calculated values for the ^{14}N hyperfine coupling very near to the experimental ones. The spin distribution is found to be on the equatorial belt of the fullerene sphere, as obtained comparing the results of the calculations with the experimentally determined ^{13}C hcc's.

From the **g** tensors of $NTEG^-$ and $TRANS1^-$ obtained at low temperature an orthorhombic symmetry for the former and an axial one for the latter have been determined. Furthermore, we have found a dependence of the *g* factors of FP radical anions on the structural rigidity of the fullerene sphere.

An anomalous dependence of the EPR line widths on the temperature for the monoadducts radicals, due to a short T_1 increasing on decreasing the temperature, has been observed, in agreement with previous results. In the present paper we have also shown that $1/T_1$ has a nearly linear dependence on T/η, and a spin-rotational relaxation mechanism is very likely to be responsible for the observed effect.

Acknowledgment. We thank prof. G. J. Moro and U. Segre for helpful discussions, dr. G. Agostini for his valuable technical support, and Mrs. E. Zangirolami for her help in the preparation of the radical anions. This work was supported in part by the CNR through its *Centro di Studio sugli Stati Molecolari Radicalici ed Eccitati*, Padova, and through Progetto Finalizzato Materiali Speciali per Tecnologie Avanzate II, and in part by MURST (cofin. ex 40%, prot. no. 9803194198) and by the European Community (TMR program USEFULL, contract No. ERB FMRX-CT97-0126).

References and Notes

(1) Kato, T.; Kodama,T.; Oyama, M.; Okazaki, S.; Shida, T.; Nakagawa, T.; Matsui, Y.; Suzuki, S.; Shiromaru, H.; Yamauchi, K.; Achiba, Y. *Chem. Phys. Lett.* **1991**, *186*, 35.

(2) Allemand, P. M.; Srdanov, G.; Koch, A.; Khemani, K.; Wudl, F.; Rubin, Y.; Diederich, F.; Alvarez, M. M.; Anz, S. J.; Whetten, R. L. *J. Am. Chem. Soc.* **1991**, *113*, 2780.

(3) Penicaud, A.; Hsu, J.; Reed, C. A.; Koch, A.; Khemani, K. C.; Allemand, P. M.; Wudl, F. *J. Am. Chem. Soc.* **1991**, *113*, 6698.

(4) Rübsam, M.; Dinse, K. P.; Plüschau, M.; Fink, J.; Krätschmer, W.; Fostiropoulos, K.; Taliani, C. *J. Am. Chem. Soc.* **1992**, *114*, 10059.

(5) Dubois, D.; Jones, M. T.; Kadish, K. M. *J. Am. Chem. Soc.* **1992**, *114*, 6446.

(6) Stinchcombe, J.; Penicaud, A.; Bhyrappa, P.; Boyd, P. D. W.; Reed, C. A. *J. Am. Chem. Soc.* **1993**, *115*, 5212.

(7) Becker, U.; Denninger, G.; Dyakonov, V.; Gotschy, B.; Klos, H.; Rösler, V; Hirsh, A.; Winter, H. *Europhys. Lett.* **1993**, *21*, 267.

(8) Subramanian, R.; Boules, P.; Vijayashree, M. N.; D'Souza, F.; Jones, M. T.; Kadisch, K. M. *J. Chem. Soc., Chem. Commun.* **1994**, 1847.

(9) Stasko, A.; Brezova, V.; Biskupic, S.; Dinse, K. P.; Schweitzer, P.; Baumgarten, M. *J. Phys. Chem.* **1995**, *99*, 8782.

(10) Stasko, A.; Brezova, V.; Rapta, P.; Asmus, K. D.; Guldi, D. M. *Chem. Phys. Lett.* **1996**, *262*, 233.

(11) Iyoda, M.; Sasaki, S.; Sultana, F.; Yoshida, M.; Kuwatani, Y.; Nagase, S. *Tetrahedron Lett.* **1996**, *37*, 7987.

(12) Sun, Y.; Drovetskaya, T.; Bolskar, R. D.; Bau, R.; Boyd, P. D. W.; Reed, C. A. *J. Org. Chem.* **1997**, *62*, 3642.

(13) Arena, F.; Bullo, F.; Conti, F.; Corvaja, C.; Maggini, M.; Prato, M.; Scorrano, G. *J. Am. Chem. Soc.* **1997**, *119*, 789.

(14) Brezova, V.; Stasko, A.; Rapta, P.; Guldi, D. M.; Asmus, K. D.; Dinse, K. P. *Magn. Reson. Chem.* **1997**, *35*, 795.

(15) Olsen, S. A.; Bond, A. M.; Compton, R. G.; Lazarev, G.; Mahon, P. J.; Marke, F.; Raston, C. L.; Tedesco, V.; Webster, R. D. *J. Phys. Chem. A* **1998**, *102*, 2641.

(16) Reed, C. A.; Bolskar, R. D. *Chem. Rev.* **2000**, *100*, 1075.

(17) Maggini, M.; Scorrano, G.; Prato, M. *J. Am. Chem. Soc.* **1993**, *115*, 9798. Prato, M.; Maggini, M. *Acc. Chem. Res.* **1998**, *31*, 519.

(18) Prato, M. *J. Mater. Chem.* **1997**, *7*, 1097. Prato, M. *Top. Curr. Chem.* **1999**, *199*, 173.

(19) (a) Maggini, M.; Karlsson, A.; Scorrano, G.; Sandonà, G.; Farnia, G.; Prato, M. *J. Chem. Soc., Chem. Commun.* **1994**, 589. (b) Liddell, P. A.; Sumida, J. P.; Macpherson, A. N.; Noss, L.; Seely, G. R.; Clrk, K. N.; Moore, A. L.; Gust, D. *Photochem. Photobiol.* **1994**, *60*, 537. (c) Belik, P.; Gugel, A.; Kraus, A.; Walter, M.; Mullen, K.; *J. Org. Chem.* **1995**, *60*, 3307. (d) Imahori, H.; Cardoso, S.; Tatman, D.; Lin, S.; Noss, L.; Seely, G.; Sereno, L.; Chessa de Silber, J.; Moore, T. A.; Moore, A. L.; Gust, D. *Photochem. Photobiol.* **1995**, *62*, 1009. (e) Williams, R. M.; Zwier, J. M.; Verhoeven, J. W. *J. Am. Chem. Soc.* **1995**, *99*, 9380. (f) Linssen, T. G.; Dürr, K.; Hirsh, A.; Hanack, M. *J. Chem. Soc., Chem. Commun.* **1995**, 103. (g) Diederich, F.; Dietrich-Buchecker, C.; Nierengrten, J.-F.; Sauvage, J. P. *J. Chem. Soc., Chem. Commun.* **1995**, 781. (h) Maggini, M.; Donò, A.; Scorrano, G.; Prato, M. *J. Chem. Soc., Chem.Commun.* **1995**, 845. (i)

Martin, N.; Sanchez, L.; Seone, C.; Andreu, R.; Garin, J.; Orduna, J. *Tetrahedron Lett.* **1996**, *37*, 5979. (j) Prato, M.; Maggini, M.; Giacometti, G.; Scorrano, G.; Sandonà, G.; Farnia, G. *Tetrahedron* **1996**, *52*, 5221. (k) Imahori, H.; Sakata, Y. *Eur. J. Org. Chem.* **1999**, 2445. (l) Martin, N.; Sanchez, L.; Llescas, B.; Perez, I. *Chem. Rev.* **1998**, *98*, 2527. (m) Guldi, D. M. *Chem. Commun*. **2000**, 321.

(20) Brustolon, M.; Zoleo, A.; Agostini, G.; Maggini, M. *J. Phys. Chem. A* **1998**, *102*, 6331.

(21) Hassan, A. K.; Pardi, L. A.; Krzystek, J.; Sienkiewicz, A.; Goy, P.; Rohrer, M.; Brunel. L.-C. *J. Magn. Reson.* **2000**, *142*, 300.

(22) Krzystek, J.; Sienkiewicz, A.; Pardi, L. A.; Brunel, L.-C. *J. Magn. Reson.* **1997**, *125*, 207.

(23) Da Ros, T.; Prato, M.; Novello, F.; Maggini, M.; Banfi, E. *J. Org. Chem.* **1996**, *61*, 9070.

(24) Kordatos, K.; Da Ros, T.; Bosi, S.; Prato, M. Manuscript in preparation.

(25) Burghaus, O.; Rohrer, M.; Gotzinger, T.; Plato, M.; Mobius, K. *Meas. Sci. Technol*. **1992**, *3*, 765.

(26) M. J. Frisch, G. W. Trucks, H. B. Schlegel, G. E. Scuseria, M. A. Robb, J. R. Cheeseman, V. G. Zakrzewski, J. A. Montgomery, R. E. Stratmann, J. C. Burant, S. Dapprich, J. M. Millam, A. D. Daniels, K. N. Kudin, M. C. Strain, O. Farkas, J. Tomasi, V. Barone, M. Cossi, R. Cammi, B. Mennucci, C. Pomelli, C. Adamo, S. Clifford, J. Ochterski, G. A. Petersson, P. Y. Ayala, Q. Cui, K. Morokuma, D. K. Malick, A. D. Rabuck, K. Raghavachari, J. B. Foresman, J. Cioslowski, J. V. Ortiz, B. B. Stefanov, G. Liu, A. Liashenko, P. Piskorz, I. Komaromi, R. Gomperts, R. L. Martin, D. J. Fox, T. Keith, M. A. Al-Laham, C. Y. Peng, A. Nanayakkara, C. Gonzales, M. Challacombe, P. M. W. Gill, B. G. Johnson, W. Chen, M. W. Wong, J. L. Andres, M. Head-Gordon, E. S. Replogle, and J. A. Pople, *Gaussian 98*, revision A.1; Gaussian, Inc.: Pittsburgh, PA, 1998.

(27) Steward, J. J. P. MOPAC93, Revision 2; QCPE: Bloomington, IN.

(28) Granovski, A. A. www http://classic.chem.msu.su/gran/gamess/index.html.

(29) Schmidt, M. W.; Baldridge, K. K.; Boatz, J. A.; Elbert, S. T.; Gordon, M. S.; Jensen, J. J.; Koseki, S.; Matsunaga, N.; Nguyen, K. A.; Su, S.; Windus, T. L.; Dupuis, M.; Montgomery, J. A. *J. Comput. Chem.* **1993**, *14*, 1347.

(30) Pfafferott, G.; Oberhammer, H.; Boggs, J. E. *J. Am. Chem. Soc.* **1985**, *107*, 2309.

(31) Pople, J. A.; Nesbet, R. K. *J. Chem Phys.* **1954**, *22*, 571.

(32) Roothaan, C. C. J. *Rev. Mod. Phys.* **1960**, *32*, 179.

(33) Dewar, M. J. S.; Hashmall, J. A.; Venier, C. G. *J. Am. Chem. Soc*. **1968**, *90*, 1953.

(34) Atherton, N. M. *Principles of Electron Spin Resonance*; Ellis Horwood PTR Prentice Hall: New York, 1993.

(35) Becke, A. D. *J. Chem. Phys.* **1993**, *98*, 5648.

(36) Lee, C.; Yang, W.; Parr, R. G. *Phys. Rev.* **1988**, *B37*, 785.

(37) Dubois, D.; Kadish, K. M.; Flanagan, S.; Haufler, R. E.; Chibante, L. P. F.; Wilson, L. J. *J. Am. Chem. Soc.* **1991**, *113*, 4364.

(38) (a) Adrian, F. J. *Chem. Phys.* **1996**, *73*, 211. (b) Tosatti, E.; Manini, N.; Gunnarsson, O. *Phys. Rev. B Condens. Matt.* **1996**, *54*, 17184.

(39) (a)Eiermann, M.; Haddon, C. R.; Knight, B.; Chan, Li, Q.; Maggini, M.; Martin, N.; Ohno, T.; Prato, M.; Suzuki, T.; Wudl, F. *Angew. Chem., Int. Ed. Engl.* **1995**, *34*, 159. (b) Knight, B.; Martin, N.; Ohno, T.; Ortí, E.; Rovira, C.; Veciana, J. H.; Vidal-Ganced, J.; Viruela, P.; Viruela, R.; Wudl, F. *J. Am. Chem. Soc.* **1997**, *119*, 9871.

(40) Brezová, V.; Staško, A.; Rapta. P.; Guldi, D. M.; Asmus, K.-D.; Dinse, K.-P. *Magn. Reson. Chem.* **1997**, *35*, 795.

(41) Brocklehurst, B.; Young, R. N. *J. Chem. Soc., Faraday Trans.* **1994**, *90*, 271.

(42) Shell-Sorokin, A. J.; Mehran, F.; Eaton, G. R.; Eaton, S. S.; Viehbeck, A.; O'Toole, T. R.; Brown, A. A. *Chem. Phys. Lett.* **1992**, *195*, 225.

(43) Eaton, S. S.; Kee, A.; Konda, R.; Eaton, G. R.; Trulove, P. C.; Carlin, R. T. *J. Phys. Chem.* **1996**, *100*, 6910.

(44) Hubbard, P. S. *Phys. Rev*. **1963**, *131*, 1155.

(45) Atkins, P. W.; Kivelson, D. *J. Chem. Phys*. **1966**, *44*, 169.